MGS accelerometer data analysis with the LMD GCM

Conference or Workshop Item

MGS ACCELEROMETER DATA ANALYSIS WITH THE LMD GCM.

M. Angelats i Coll, F. Forget, *Laboratoire de Meteorologie Dynamique, CNRS, Universite Paris 6, Paris.***, M.A. Lopez-Valverde,** *Instituto de Astrofisica de Andalucia, Granada, Spain***, P.L. Read, S.R. Lewis,** *Atmospheric, Oceanic and Planetary Physics, University of Oxford***.**

Introduction

Mars Global Surveyor aerobreaking phases, required to achieve its mapping orbit, have yielded vertical profiles of thermospheric densities, scale heights and temperatures covering a broad range of local times, seasons and spatial coordinates [*Keating et al.* 1998, 2001]. Phase I covered local times from 11 to 16 h (assuming 24 "martian hours" per martian day or sols), with a latitude coverage of approximately 40° to 60°N. Seasons observed during this phase were centered around winter solstice and altitudes of periapsis range from 115 to 135 km. The altitudes for Phase II were lower, with a minimum around 100 km and a maximum around 120. Martian spring was the season covered during this phase and the local time was between 15 and 16 h. The latitude covered by Phase II, however, was more extense than that seen during Phase I, with a coverage from 60°N to basically the South Pole.

MGS density data above 110 km as sampled at a fixed local time yield large amplitude longitudinal variations composed of a variety of wavenumbers (s) which are characterized by large $s = 2$ component and smaller $s = 1$ and $s = 3$ contributions. These oscillations were first interpreted as possible stationary planetary waves [*Keating et al.* 1998], while it has been later suggested that eastward propagating waves of diurnal frequency could be responsible for the density signature [*Forbes and Hagan*, 2000;*Wilson*,2000].

A fixed local time sampling of the atmosphere will yield a signature composed of a variety of different waves. Determining the dominant ones can be an impossible feat from the observations alone. Waves that propagate with the apparent motion of the sun and have periods that are subharmonics of a day (i.e. the migrating tides) will yield a constant value and no longitudinal variation when sampled at a fixed local time. Only nonmigrating tides will contribute to a longitudinal structure at a given local time.

By nonmigrating tides, one refers to those oscillations that have periods that are subharmonics of a day, but their phase speed ($\frac{\sigma}{s}$) differs from the migrating tide's value of $\frac{2\pi}{24}$ (h^{-1}). These oscillations, in contrast to the westward migrating tides, can have eastward or westward propagation with respect to the sun, or be standing. Nonmigrating tides can be directly forced, or arise as the outcome of a nonlinear interaction between other preexisting waves.

GCM Simulations and MGS Data Comparisons:

The Mars LMD GCM has evolved from a terrestrial climate model [*Hourdin et al.*, 1993;*Forget et al.*, 1999] and has been extended to the Mars upper atmosphere through a collaboration with the University of Oxford and the Instituto de Astrofísica de Andalucía. The model extends from the ground up to a height of approximately 120 km and includes the relevant processes near the surface such as turbulent diffusion in the planetary boundary layer, convection, orography and low-level drag, all at sub-grid scales. The energetics of the simulations include the effects of the presence in the Mars atmosphere of dust and CO_2. Parameterizations of thermal infrared cooling and near-infrared heating by CO_2 both account for non-LTE effects. The CO_2 condensation-sublimation cycle is also realistically included. A more detailed description of the model can be found in *Forget et al.* [1999].

MGS Accelerometer observations used in this analysis are NASA Level 3 data set consisting of atmospheric properties at constant altitude levels for each orbital pass covering from 130 to 160 km height [*Keating et al.*, 2001]. Given that lower altitudes were required since our model simulations don't reach such heights, periapsis density data was scaled to the four following levels: 110, 115, 120 and 130 km. This latter height was only obtained for the orbits that had periapsis altitude above 122 km. Data was sorted according to common local times at each altitude and the profiles obtained, where a significant number of points was available, are shown in Figure 1 along with GCM results that correspond to the observations.

In general, model simulations are able to reproduce the observations with very good agreement. Notable agreement is found at 115 km for the northern spring seasons of Ls=30°-60° (Figure 1a) and Ls=60°-90° (Figure 1e). For these two cases the wave structure observed from orbit is clearly reproduced in the GCM data, and seems to be strongly composed of wavenumbers 2 and 3. Comparisons at Ls=60°-90° reveal a latitudinal dependence, with lesser agreement with the observations in the southern hemisphere as the latitude becomes more poleward. This can be seen in Figure 1b to 1d. A plausible explanation for this discrepancy is the large day-to-day variability that is found to exist at high southern latitudes above 90 km in the GCM simulations. The positioning of this highly variable region over the top of the eastward zonal jet is suggestive of a baroclinic instability generating some of the wave activity present there. At 130 km

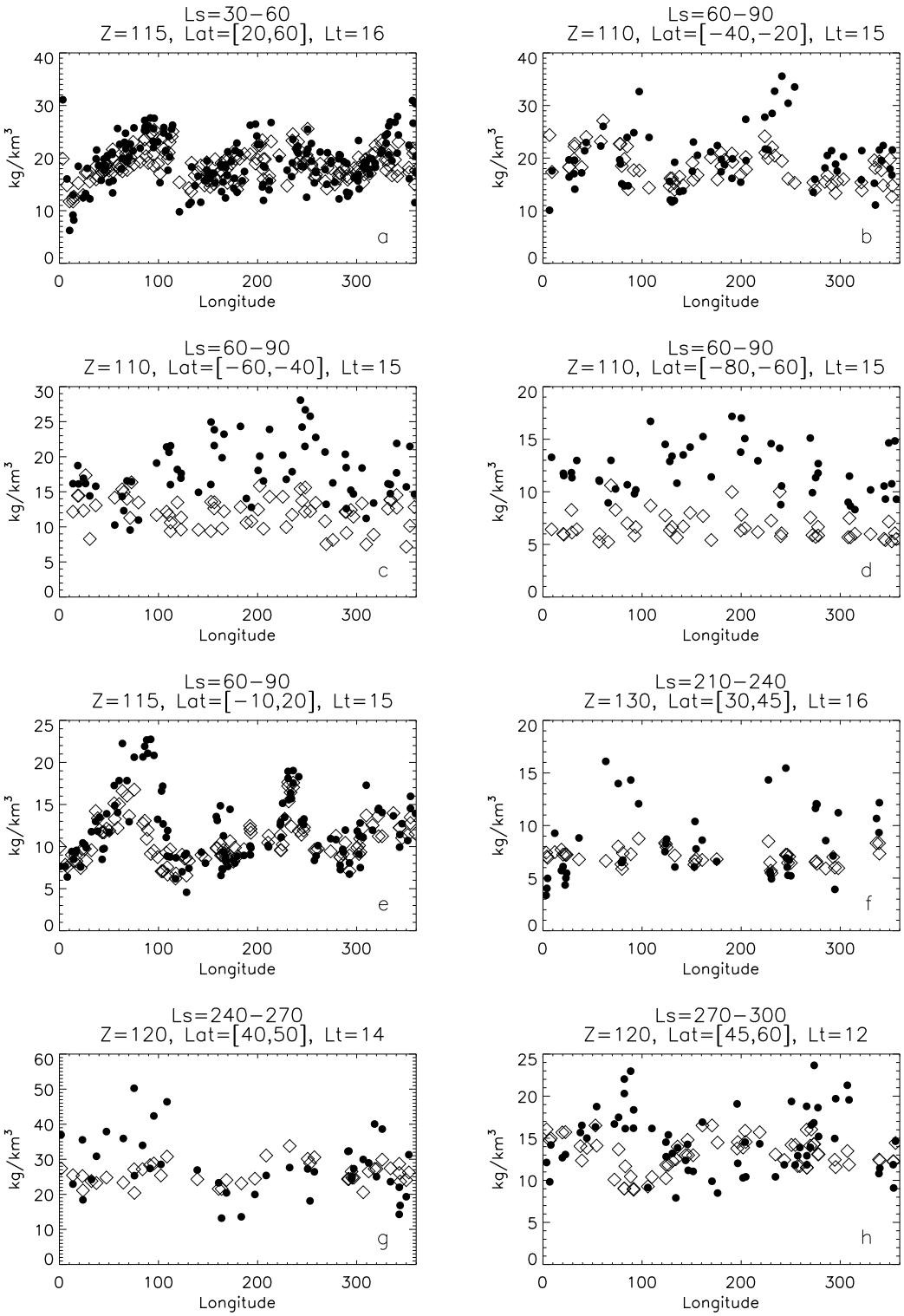

Figure 1: MGS versus LMD GCM density comparison. MGS data interpolated at the altitude Z (above the grid) are represented with solid dots, while GCM results obtained at the same location and time are displayed in diamonds. Units are kg/km^3. Season, time and location are marked for each panel.

(Figure 1f), some of the differences could be ascribed to the high altitude of the observations, this being almost the limit of the valid simulation data. Figures 1g and 1h show comparisons at 120 km during two dusty seasons around northern winter solstice. The agreement with the observations is rather good and slight differences can possibly be due to regional dust storm properties of the period.

Wave Analysis

Given the rather striking agreement obtained between MGS data and the GCM simulations for the same conditions, an analysis of the modeled data can shed some light on the wave activity at work in the upper atmosphere of Mars. The focus of our analysis is on Phase II MGS accelerometer data. These observations correspond to orbits 582 to 930 which saw a progression of aerocentric longitude from $Ls = 33°$ to $Ls = 73°$. For this orbit period, the latitude of periapsis saw a southward progression from 60°N to approximately 20°S. The local solar time sampled a two-hour bracket from 17 to 15 h. Specifically, Figure 1e represents equatorial latitudes (10° S-22° N) at a height of 115 km for $Ls \approx 70°$, which correspond to a local time of 15 h. As can be seen, a very good agreement with the observations is obtained with the wave structure clearly represented. The data shows a possible combination of wavenumber 2 and 3 as seen in a fixed local time frame of reference.

Such kind of structures have been observed and interpreted as stationary waves [*Keating et al.*, 1998] and have later been shown to be nonmigrating tides, and more specifically, diurnal Kelvin Waves [*Forbes and Hagan*, 2000; *Wilson*, 2002]. The excitation mechanism for these eastward waves has been suggested to lie in the nonlinear modulation of the migrating diurnal tide forcing by Mars' topography components [*Wilson and Hamilton*, 1996; *Forbes and Hagan*, 2000]. A wave analysis of the LMD GCM simulation data yields other significant contributors to the structures observed by MGS.

A two-dimensional Fourier decomposition was performed on the GCM data to extract the prominent waves present. The analysis was performed on ten days of simulation with wavenumbers ranging from -10 to 10 (westward and eastward, respectively) and periods from 8 to 72 hours. Stationary waves with wavenumbers 1 to 6 were also examined. The obtained density amplitudes for the different wavenumbers normalized by the zonal mean density are depicted in Figure 2 corresponding to diurnal frequencies. Magnitudes are largest for the migrating tide, with significant amplitudes obtained for the diurnal eastward propagating waves with $s = 1, 2$ and 3. Lesser amplitudes are found for shorter and zonally symmetric waves. Semidiurnal nonmigrating tides (not shown) have in general smaller amplitudes than those of

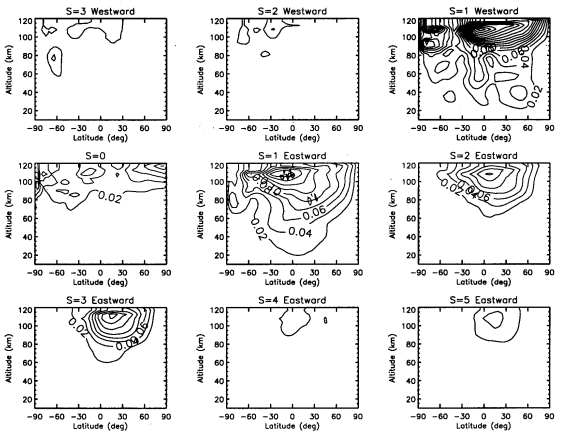

Figure 2: Relative density amplitude at $Ls \approx 70$ for diurnal frequency waves. Amplitudes are normalized by local zonal mean values. Wavenumbers range from -3 (westward) to 5 (eastward). Contour intervals are 0.02.

diurnal frequency, with the $s = 1$ and zonally symmetric ($s = 0$) waves found to maximize above 80 km at high northern latitudes. Significant magnitudes are also seen at wavenumbers two, three and five for the eastward propagating semidiurnal waves.

The largest amplitudes for nonmigrating tides are obtained for eastward propagating diurnal waves with wavenumbers one, two and three (with magnitudes of 1.36, 0.99, and 1.17 respectively). Their contribution to the wave structure seen in fixed local time in Figure 1e is shown in Figure 3. The three components are depicted along with their total sum in comparison with the GCM simulation data corresponding to the MGS data of Figure 1e. GCM data is here presented without contributions from the zonal mean nor migrating tides. This contribution is individually calculated for each point as the longitudinal mean at a given local time and latitude. The eastward propagating diurnal waves provide a significant portion of the structure, accounting for approximately 50% of the maxima values. The addition of stationary wave one, two and three (not shown) does not increase significantly the closeness of the decomposition. The spike observed at 230°E longitude and nicely reproduced on the simulated data (Figure 1e) shows a significant contribution from the eastward propagating waves ($\sigma = 1/12, s = 2$), ($\sigma = 1/12, s = 5$), and ($\sigma = 1/24, s = 5$). Their contribution to the observed structure is seen in Figure 3, where they have been added to the eastward diurnal s=1,2,3 waves. As can be seen, the agreement is significantly improved with the addition of these three waves.

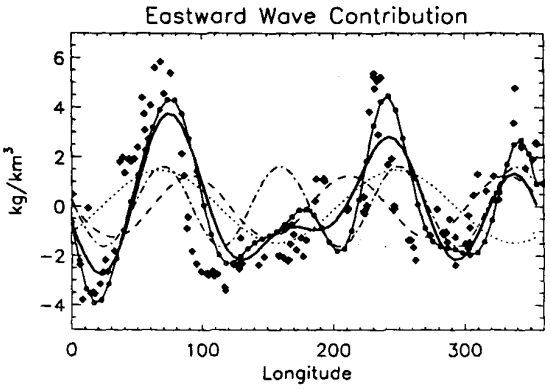

Figure 3: Contribution to wave structure from the eastward propagating $s = 1, 2$ and 3 diurnal oscillations. Black diamonds correspond to GCM simulations for $Ls \approx 70$ at LT=15 and 115 km for the equatorial band covered by MGS observations (10S-20N) with zonal mean and migrating tides subtracted. Waves are shown as follows: dotted, $s = 1$; dashed, $s = 2$; dash-dotted, $s = 3$; solid, sum of the three. Solid line with circles is as solid line with eastward semidiurnal s=2 and 5 and diurnal s=5 added.

Summary

LMD GCM simulations have been used to study aerobraking accelerometer data from MGS for various seasons, altitudes and latitudes. In general, the model simulations fare very well in the comparison with the observed data which allows for its use its analysis. Results show better agreement at mid to low latitudes, while high latitude comparisons present larger differences between the modeled and observed data. These differences are ascribed to the high day-to-day variability obtained at high latitudes in the simulated data. This transient behaviour has to be further studied and will be addressed in a separate analysis. Dusty season results reproduce the main features observed by MGS, although few discrepancies are thought to relate to differences in the dust distribution in the simulations.

We have focused on MGS data, obtained at constant local time for Ls=70° at an altitude of 115 km. These observations are well reproduced in the LMD GCM. The model clearly simulates the planetary-wave structure seen in the observed data. The sampling at a single local time of waves in the atmosphere renders impossible the extraction of the different wave components from the observations since a variety of wavenumber-frequency combinations can yield a certain signature when sampled at a constant local time. This makes the use of model simulations an invaluable tool in the understanding of observations.

Two-dimensional Fourier decomposition of the simulation data yields the diurnal eastward propagating waves with wavenumber one, two and three as the major contributors to the structure observed by MGS at equatorial latitudes. Other significant waves obtained are the semidiurnal eastward propagating waves with wavenumbers two and five which along with the diurnal $s = 5$ help create the strong signature at a longitude of 230°E seen in the data. It is striking that such a combination of minor waves can increase the density encountered by a spacecraft by almost 40%. This illustrates the complex nature of the Martinan atmosphere at those heights and the need for further observations and continuing modelling efforts.

Acknowledgements

This research was funded under cNES Mars Premier Program and ESTEC Contract 11369/95/NL/J.

References

[1] Forbes, J., and M. Hagan, Diurnal kelvin wave in the atmosphere of Mars: Towards an understanding of 'stationary' density structures observed by the MGS accelerometer, *Geophys. Res. Lett., 27*, 3563–3566, 2000.

[2] Forget, F., et al., Improved general circulation models of teh martian atmosphere from teh surface to above 80 km, *J. Geophys. Res., 104*, 24155–24176, 1999.

[3] Hourdin, S., et al., Meteorological variability and the annual surface pressure cycle on Mars, *J. Atmos. Sci., 50*, 3625–3640, 1993.

[4] Keating, G., et al., The structure of the upper atmosphere of Mars: In situ accelerometer measurements from Mars Global Surveyor, *Science, 279*, 1672–1676, 1998.

[5] Keating, G., et al., MGS-M-ACCEL-5-ALTITUDE-V1.0, *NASA Planetary Data System*, 2001.

[6] Wilson, R., Evidence for diurnal period kelvin waves in the martian atmosphere from Mars Global Surveyor TES data, *Geophys. Res. Lett., 27*, 3889–3892, 2000.

[7] Wilson, R., Evidence for nonmigrating thermal tides in the Mars upper atmosphere from the Mars Global Surveyor Accelerometer Experiment, *Geophys. Res. Lett., 29*, 2002.

[8] Wilson, R., and K. Hamilton, Comprehensive model simulation of thermal tides in the martian atmosphere, *J. Atmos. Sci., 53*, 1290–1326, 1996.